



University of HUDDERSFIELD

University of Huddersfield Repository

Molyneux-Berry, Paul and Bevan, Adam

Wheel surface damage: relating the position and angle of forces to the observed damage patterns

Original Citation

Molyneux-Berry, Paul and Bevan, Adam (2012) Wheel surface damage: relating the position and angle of forces to the observed damage patterns. *Vehicle System Dynamics*, 50 (S1). pp. 335-347. ISSN 0042-3114

This version is available at <http://eprints.hud.ac.uk/id/eprint/16025/>

The University Repository is a digital collection of the research output of the University, available on Open Access. Copyright and Moral Rights for the items on this site are retained by the individual author and/or other copyright owners. Users may access full items free of charge; copies of full text items generally can be reproduced, displayed or performed and given to third parties in any format or medium for personal research or study, educational or not-for-profit purposes without prior permission or charge, provided:

- The authors, title and full bibliographic details is credited in any copy;
- A hyperlink and/or URL is included for the original metadata page; and
- The content is not changed in any way.

For more information, including our policy and submission procedure, please contact the Repository Team at: E.mailbox@hud.ac.uk.

<http://eprints.hud.ac.uk/>

Wheel surface damage: relating the position and angle of forces to the observed damage patterns

Paul Molyneux-Berry, Adam Bevan

Rail Technology Unit. Division of Mechanical Engineering

Manchester Metropolitan University, John Dalton Building

Chester Street, Manchester, M1 5GD, England

e-mail address of corresponding author: p.molyneux-berry@mmu.ac.uk

Wheel surface damage: relating the position and angle of forces to the observed damage patterns

A new method of presenting simulated wheel/rail forces and relating these to observed wheel damage has been developed. This indicates good correlation between the predicted forces and the regions of the wheel where damage is observed in practice. There is also good correlation between the angle of the predicted forces and the observed cracks. The angle evidence suggests that the dominant RCF cracks on field side of the wheel tread are initiated by the occasional high forces when the opposite wheel is running in flange contact on sharp curves. Cracks may then be propagated by more frequent lower forces on moderate curves.

Keywords: wheel damage; rolling contact fatigue; contact force; position; angle

1. Background

Improvements in rail vehicle suspension design, and the introduction of disc brakes and wheel slide protection systems, have tended to reduce wheel wear and the incidence of flats. Wheel turning intervals are now longer and often limited by wheel fatigue damage mechanisms which did not have a chance to develop previously. Such damage can appear as cavities, shelling, spalling, and rolling contact fatigue (RCF) cracks.

These mechanisms have been studied by several authors [1, 2, 3] and various simplified models have been proposed. However, none can fully represent the complexity of the real world wheel/rail interface, and consequently are of limited applicability to practical problems in optimising wheelset maintenance. Nevertheless, simplified models can be very useful if their validity is proven by comparison with real observed data.

Recent work has reviewed trends of wheel damage in the UK passenger rolling stock fleets [4]. Many factors influence damage on a particular wheel, and other issues

affect the accuracy of damage observations. Consequently, the datasets contain wide scatter: a challenge for validation of wheel damage mechanism models.

However, there are more consistent trends in the position and nature of the observed wheel damage. The objective of this paper is to associate the observed damage types and locations with the vehicle running conditions that cause them. It is hoped that this will lead to the development of improved damage models, and a better understanding of possible measures to reduce wheel damage in practice.

2. Observations

The initial basis of this work was a dataset of wheel damage observations from a modern diesel multiple unit fleet, gathered as part of a previous project. The fleet exhibits a variety of damage types and the crack patterns on motored and trailer wheels are significantly different. This monitoring exercise is currently being extended to record the damage patterns observed on 36 wheelsets throughout their life, and to relate this to the operational duty cycle. Crack observations from other fleets have also been considered where appropriate.

The wheels on the monitored fleet are of forged R8T steel, rim-quenched and tempered. This manufacturing process induces circumferential compressive stresses in the rim, and a degree of surface hardening. These stresses and material properties are also influenced by work-hardening in service, and by removal of material by wear and on the wheel lathe. Such variations are likely to influence the initiation and propagation rates of RCF cracks; they have not been directly considered in this paper which focuses more on the location and pattern of RCF cracks. Residual stresses and hardness variations in wheels of this fleet are the subject of ongoing research by the authors of this paper, and it is hoped to publish the results in due course.

On the observed fleet of vehicles, RCF cracks on the wheels of trailer axles are typically toward the field side of the wheel tread (i.e. furthest from the flange). Typically, they occur at an angle of about 135° relative to the direction of motion - *Figure 1(a)*. They are usually uniform around the wheel circumference, but sometimes appear in patches. Often the cracks are slightly curved, being closer to circumferential near the field side, and closer to transverse toward the centre of the tread - *Figure 1(b)*. This photo also shows the cavities formed at a later stage of crack development. Below the surface, the cracks angle down into the material and there may be several cracks overlaid - *Figure 1(c)*, which shows a sectioned wheel. The sharp edges which can be felt on the surface give an indication of the sub-surface direction of the crack.

The trains in the observed fleet run on routes with an even distribution of left and right hand curves. They also run equal distances in both directions, so each wheelset spends half of its life leading the bogie, and half trailing. The observed patterns of damage are therefore usually mirror-symmetrical on a bogie.

Wheels on powered axles on the observed fleet show a different damage pattern, with a field-side band of circumferential cracks - *Figure 1(d)*. These are usually less severe than the angled cracks on the trailer axles; they can be quite obvious on the surface but do not usually propagate deep into the material.

A second band of cracks can initiate close to the flange root; usually these do not propagate into the wheel, but can be seen and felt - *Figure 1(e)* on a powered axle, and *Figure 1(f)* on a trailer axle.

Transverse surface cracks in the centre of the tread are occasionally seen on other fleets - *Figure 1(g)* - especially where high braking forces occur, but they are not seen on the monitored fleet. Isolated sub-surface transverse cracks occasionally appear in this region of the tread; these are similar to the 'squats' sometimes observed in rails.

The low tangential forces associated with contacts on this part of the wheel mean that the peak stress is below the surface. The relatively low stresses are not usually sufficient to initiate cracks, but the large number of stress cycles can cause existing material flaws to propagate. One wheelset with this type of damage has been seen on the monitored fleet, but the cracks were only discovered during routine turning of the wheelset on the lathe.

Wheel tread cracks can be associated with other forms of damage, including thermal damage from wheel slide incidents causing patches of brittle martensite. Cracks can also propagate from indentations in the wheels - *Figure 1(h)*.

The damage observed on a wheel is accumulated from operation in many different conditions. Rail damage mechanisms are better documented and understood because rails experience much more consistent forces: they are installed on a particular curve radius, usually with fairly uniform traffic in terms of vehicle type, speed and direction. In comparison, wheels experience a full range of curves, speeds, traction/braking, and running direction. With such a variety of conditions, the inter-relationship between different damage mechanisms such as wear and crack growth is more significant on wheels.

The difference in the observed nature and rate of formation of RCF damage on powered and unpowered wheels on this fleet demonstrates that traction and braking forces have a significant influence on wheel RCF. Similar behaviour has also been observed by the author on other fleets as part of research work for the Rail Safety and Standards Board. It is therefore essential to model these forces in any simulations intended to predict RCF damage.

On many UK passenger multiple-unit fleets, the leading wheelsets of the trains suffer more rapid RCF damage, and again this is borne out by the present monitoring

programme. Leading wheelsets are often more prone to wheel slide events, and resulting weakened or embrittled material may promote the initiation of cracks. Additionally, leading wheelsets are more likely to have fluids or other contaminants present in the wheel/rail contact. These may promote crack propagation, or reduce the levels of wear that might otherwise remove cracked material. However, the implications of these effects are not fully understood at present.

Another general observation is that smaller diameter wheels (near end of life) suffer more rapid RCF damage. This appears to be true for several UK passenger fleets. Smaller wheels will have higher contact stresses and more wheel rotations for a given distance run, but these effects are probably less significant than the change in material properties through the depth of the wheel. Residual compressive stresses in the wheel rim provide some protection against crack propagation, and these stresses may be lower in a wheel near the end of its life. Again, the implications of these effects are not fully understood at present, but future work is planned to examine the material properties and residual stress through the cross-section of several wheel samples, including new and life-expired examples from the monitored fleet.

3. Simulations

Dynamic simulations have been used to predict the wheel/rail contact conditions and forces for the monitored vehicles, running on the 68km route where they operate most frequently. Vampire® vehicle dynamics software has been used, and the inputs were made as accurate as possible using currently available data. These included:

- Track geometry measured from a track recording car
- Flange face friction reduced locally at track-side lubricator locations
- Speed profiles based on on-train data recorder information

- Traction and braking forces based on on-train data recorder information
- 8 measured rail profile pairs applied according to curve radius bands
- 9 wheel profile pairs measured from the vehicles in varying wear states

It is hoped that future simulations will use a much larger number of the actual rail profiles measured on the route, as this functionality has now been added to the track recording car. It is also intended to extend the simulations to cover the entire network operated by these vehicles. Simulation outputs were selected to characterise the wheel/rail contact conditions. The main parameters considered to date are as follows:

- size of the contact patch and its position on the wheel tread
- direction of the net tangential force
- normal and tangential contact stress
- $T\gamma$, the energy dissipated in the contact patch

4. Comparison of observations and simulation results

Plotting methodology

A new technique has been developed using Matlab® for processing and plotting the wheel/rail contact parameters on a single circular plot, for comparison with observations. A particular simulated contact condition is indicated by a coloured spot:

- The angular position Ψ on the circular plot represents the angle of the creep force on the wheel, relative to a datum forwards along the rail - *Figure 2(a)*. This angle is measured in the contact plane, which is nearly horizontal for tread contacts where wheel RCF usually occurs.
- The radial position y on the circular plot represents the contact position across the wheel tread, as indicated by the superimposed wheel profile - *Figure 2(b)*.

- The colour of the spot is used to indicate the magnitude of the damage parameter. In *Figure 2(b)*, the spot is large but when plotting an entire route, small spots are used to avoid data being hidden. Additionally, the data is plotted in order of increasing damage value, so that where multiple contacts are overlaid, the highest (and probably most damaging) value is visible.
- For the 68km route, the spots are output at intervals of approximately one wheel revolution, and therefore can be visualised as the history of damage at one location on the rim of each wheel. This resolution of approximately 3m is sufficient to capture most wheel/rail interaction effects on plain line, while keeping data volumes manageable.

Observed crack damage can be plotted on the same figure as a series of lines: different bands of damage on the wheel are shown as black radial lines at the appropriate radial position on the plot. For observed damage, the plotted angle of the lines is normal to the surface crack direction - *Figure 2(c)*. There are two possible normal directions to a crack, but by feeling for sharp edges on the surface of the wheel, the subsurface direction of the crack can be determined, and this can be related to the direction of the forces that propagate the crack.

Plots of $T\gamma$ related to wear and RCF damage

Figure 3 shows an example set of circular plots, representing the $T\gamma$ values predicted on all four wheels of the powered bogie for a 68km route. The leading wheelset of the bogie is shown in the upper plots, and the trailing wheelset in the lower plots.

A colour scale has been chosen to highlight the most damaging ranges of $T\gamma$, based on the $T\gamma$:damage relationship in the Whole Life Rail Model (WLRM) [5].

According to the WLRM, contacts with $T\gamma < 15$ have insufficient energy to generate

damage; these are therefore omitted for clarity. $T\gamma$ values likely to cause purely RCF damage according to the WLRM ($15 < T\gamma < 65$) are shown with shades of yellow through orange, while red represents the peak of the WLRM damage function at $T\gamma = 65$. Beyond this value, the likelihood of initiating RCF damage and the crack propagation rate are counteracted by wear from the material surface; this regime is indicated by the shades of purple and blue. For $T\gamma > 175$, the WLRM function suggests that damage is entirely in the wear regime and this is shown in green.

Looking at Figure 3, a clear pattern of predicted forces is immediately apparent. As described above, the simulation includes a wide variety of input conditions (curve radii, wheel/rail profiles, traction/braking, friction coefficient etc) yet the contacts with predicted damaging $T\gamma$ values are clustered in distinct areas of the circles, each region with a characteristic colour range indicating the nature of the damage that would be predicted by the WLRM. The patterns of damage are very similar on left and right hand sides, because the route has a balanced distribution of left and right hand curves.

Observed cracks are also shown: toward the field side these are predominantly near-circumferential ($90^\circ < |\Psi| < 120^\circ$) but there are also some small cracks near the flange root at $|\Psi| \approx 45^\circ$. Owing to the symmetry of the vehicle operation and damage observations, the observed cracks are plotted on all four wheels of the bogie, with their locations mirror-symmetric as observed in practice. The two bands of observed cracks may appear parallel - *Figure 1(f)* - but appear opposite each other on the circle owing to their sub-surface propagation directions (identified by feeling the surface of the wheel) and are therefore likely to be caused by forces in the directions shown.

To illustrate the running conditions that cause contact in each of the regions of the plot, Figure 4 shows the results from running on a right-hand spiral curve, at balance

speed with no traction or braking forces, no track irregularities, and a single wheel/rail profile combination. The track input conditions are shown in Figure 5.

The same damage parameter scale is used, but in this case all values of $T\gamma$ are shown, with the non-damaging values of $T\gamma < 15$ in a pale yellow colour.

The curve radii are also annotated on Figure 4: Blue figures indicate tread contacts and black figures are flange contacts. For this combination of wheel and rail profiles, $T\gamma$ exceeds 15 on both leading wheels at about 1500m radius, and $T\gamma = 65$ at 900m radius. The outer flange comes into contact at about 600m radius, and on the leading wheelset $T\gamma$ reaches 175 at about 300m radius. The trailing wheelset only experiences damaging $T\gamma$ values on curves sharper than 300m radius, and enters flange contact (on the inner wheel) at about 120m radius.

For comparison with Figure 3, the sharpest curve on the 68km route is 250m radius and the majority of the curves are around 1000m radius. However, the presence of track irregularities can give sharper local curvatures, and the wheel/rail forces are also influenced by traction and braking forces and a wider range of wheel/rail profile combinations.

Relationship between simulated contact conditions and observed damage

The two regions of observed cracking shown in Figure 3 correspond with regions of predicted damaging forces on the leading wheelset. Forces on the trailing wheelset are lower, and do not occur at positions or angles corresponding to the observed damage. It is notable that the regions of observed tread RCF damage typically correlate with the areas of higher forces ($75 < T\gamma < 175$ or $1.5 < T\gamma/\text{Area} < 3.0$), and Figure 4 confirms that these usually occur when running in or near flange contact on sharper curves. This is in contrast to the current rail RCF model where the peak damage occurs at $T\gamma = 65$ for

standard R260 rail steel material [6]. The key regions where damaging forces are predicted are shown on Figure 6 and discussed in more detail below.

Region 1: Contact in the centre of the wheel tread

On straight track, the wheelset tends to run centred between the rails, and the wheel/rail contact is close to the nominal position, 70mm from the flangeback. Under these conditions, the creep forces are generally below the damage threshold but those appearing in the plot coincide with heavy brake applications (Ψ close to 180°).

For most vehicle types including the monitored fleet, these conditions are rare but this type of damage - *Figure 1(g)* - is occasionally seen on locomotives.

Region 2: Flange Root Contact

When the vehicle is running on a large radius left hand curve, the leading right hand contact moves towards the root of the flange. The rolling radius difference generates a forwards force, while the angle of attack generates a lateral force to the right. The resultant creep force acts at approximately 45° . On sharper curves, the contact moves towards the flange and the creep forces rise, giving higher $T\gamma$ values.

In this region of the circle plot, the direction of the longitudinal force on the wheel is forwards. This tends to force closed any cracks in the wheel before they enter the contact patch - *Figure 6(b) top right* - and thus reduces the opportunity for fluid entrapment and the associated crack propagation mechanisms. This correlates with the observed damage - *Figure 1(e),(f)* - which features fine surface cracks with no significant depth. These contact conditions can however cause serious RCF in rails.

Region 3: Flange Contact

On sharp curves, there is a transition from Region 2 into flange contact. High $T\gamma$ values are generated on the flange face. The angle co-ordinate of the flange contact can appear misleading as it is measured in the (inclined) flange contact plane. However, flange face damage is generally wear, which is not sensitive to force angle.

Flange contacts usually occur on sharper curves and the wear rate is heavily dependent on the presence and effectiveness of lubrication under such conditions. The observed fleet exhibits mild flange wear, but this does not drive wheel turning intervals or have a great influence on the material removed at turning.

Region 4: Two-Point Contact

Many combinations of wheel and rail profiles have a zone of 2-point contact (tread and flange). One contact is predicted in region 3, and a second contact in region 4. For a given wheel/rail profile combination, these contacts will always be at the same locations on the tread and flange, so Region 4 on the circle plot is characterised by a series of arcs at a constant radius. Taking into account the contact patch size, these arcs would merge.

The differing velocities in the two contacts cause high creep forces and hence high $T\gamma$ as shown. However, these conditions occur infrequently, and the crack angles observed on the wheel in this location suggest that they are caused by forces in Region 2, rather than Region 4.

Region 5: Low Rail Contact (moderate curves)

Running on a large radius right hand curve, the leading right hand contact is on the low rail. The wheelset is offset laterally towards the high rail (contacting in Region 2) while the contact on the low rail is toward the field side of the tread (Region 5). The resulting rolling radius difference gives a component of creep force in the backwards direction,

which steers the wheelset towards a radial position. However, the wheelset is constrained by the suspension and therefore retains an angle of attack to the rail. This generates a component of creep force tending to pull the wheel away from the low rail. The resulting net creep force acts at approximately -160° , as shown in Region 5. As the curves become sharper, the contact moves further towards the field side (outwards) and the lateral creep forces rise, giving higher $T\gamma$ values at larger angles.

In this region of the circle plot, the direction of the longitudinal force on the wheel is backwards. This tends to force open any cracks in the wheel before they enter the contact patch - *Figure 6(b) bottom right* - and thus promotes fluid entrapment and the associated crack propagation mechanisms. This correlates with the damage on the trailer axles of the observed fleet - *Figure 1(a),(b)* - which feature cracks that propagate to a significant depth, and associated cavities - *Figure 1(c)*.

Region 6: Low Rail Contact (sharp curves)

This region is a continuation of Region 5 for sharper curves; it corresponds to conditions where the opposite wheel is in flange contact. The low wheel contact moves further towards the field side (outwards) and the lateral creep forces (gauge spreading forces) rise significantly, giving still higher $T\gamma$ values at larger angles. This correlates with the damage on the motor axles of the observed fleet - *Figure 1(d)* and the band on the right of *Figure 1(e)* - where the combination of higher primary suspension yaw stiffness and traction forces brings the creep force angle close to -90° (lateral).

The predominance of circumferential RCF cracks in this region on the motored axles suggests that the high lateral forces under such conditions may be responsible for initiating the cracks. These may then be propagated by the more frequently encountered forces in Region 5.

Plots of contact stress

The circular plotting method can also be applied to other forms of wheel damage parameter including $T\gamma/\text{area}$, contact stress, or shakedown exceedence. Figure 7 is an example plot showing normal contact stress; in this case the peak Hertzian stress calculated from the same Vampire® simulations used for Figure 3. Whilst elastic elliptical contacts are a simplification of the real behaviour, they are reasonably accurate for contacts on the wheel tread where the dominant RCF damage is observed.

The majority of peak contact stresses are below 1.5GPa but there are some regions with higher stresses up to 2.5GPa; these high values are mostly associated with the damaged regions of the wheel. Such high stresses would in practice be relieved by plastic flow and would contribute to wear or fatigue damage in the wheel material.

It appears that the fatigue damage observed on the wheel occurs in regions where both the $T\gamma$ and the contact stress are high, even though these conditions are relatively uncommon.

Behaviour on Switches and Crossings

Figure 8 shows circular damage plots of predicted $T\gamma$ values (similar to Figure 3), representing the behaviour when running over switches and crossings. Whilst turnouts represent only a small proportion of the total distance run by these vehicles, the varying rail profiles can give quite different contact conditions. The rolling radius of the wheel changes rapidly as the load is transferred from switch to stock rail or crossing nose to wing rail, and this can generate high tangential forces. This simulation was carried out to identify whether the conditions experienced on switches and crossings are likely to contribute to the observed wheel damage.

A selection of turnout geometries was considered, including facing and trailing switches on normal and diverging routes. The switch was represented with 36 rail profile cross-sections, and 21 profiles were used for the crossing. Although the Vampire® approach of interpolating between wheel/rail contact data is not ideal for this application, the number of profiles considered should minimise any associated errors. To capture the influence of the rapidly changing contact conditions on switches and crossings, the coloured spots representing the contact conditions are output at intervals of 0.1m on Figures 8 and 9.

Compared to Figure 3, Figure 8 shows a different pattern of predicted forces, with the dominant contacts closer to the flange root, and significantly higher T_y values on the trailing wheelset.

The turnouts simulated represent the most common type in the UK, which have a vertical rail profile throughout rather than the 1:20 inclined rail used on plain line. This means that the contact patch tends to be closer to the wheel flange, and therefore does not align with the dominant band of wheel RCF damage. However, there are significant predicted damaging contacts in the region of the secondary crack band near the flange root – *Figure 1(e),(f)* – and it is possible that the interactions on switches and crossings contribute to this form of damage.

Figure 9 plots the contact stress for the same simulation. Compared to the plain line case on a 68km route - *Figure 7* - the stresses are much higher, with many contacts exceeding 2500 MPa. This is likely to be influenced by the small rail profile radius on the switch toe and crossing nose giving a small contact patch, combined with impact loads as the wheels transfer onto these rails. In reality, such high stresses would probably be relieved by plastic flow and would contribute to wear or fatigue damage in

the wheel material. This behaviour affects both leading and trailing wheelsets in a similar way.

These results suggest that wheel/rail interactions on switches and crossings do not have a great influence on the dominant band of observed wheel RCF. However, the high normal and tangential forces applied to the flange root area may contribute to the observed damage in this region of the wheel.

5. Conclusions

A new method of presenting simulated wheel/rail forces and relating these to observed damage has been developed. This indicates a good correlation between the predicted high forces and the regions of the wheel where wear or fatigue damage is observed in practice. There is also good correlation between the angle of the predicted forces and the observed cracks.

The angle evidence suggests that the dominant RCF cracks on field side of the wheel tread are initiated by the occasional high forces ($75 < T\gamma < 175$ or $1.5 < T\gamma/\text{Area} < 3.0$) when the opposite wheel is running in flange contact on sharp curves. This is in contrast to the current rail RCF model[6] where the peak damage rate occurs at $T\gamma = 65$, and occurs on moderate curves generally without flange contact.

Cracks may then be propagated by more frequent lower forces on moderate curves. It is hoped to confirm this with continuing detailed wheel damage observations, and by adding further detail to the simulations.

If running in flange contact is a key driver of wheel RCF initiation, there is a risk that the implementation of rail grinding and adoption of anti-RCF wheel profiles (to avoid contact in Region 2 and hence rail RCF) may cause increased rates of wheel RCF. This will be investigated further in future work.

Analysis of the Hertzian contact stress suggests that high normal stresses also correlate with the regions of observed crack and wear damage on the wheels. Future work will aim to investigate whether a damage model could be developed based on a combination of T_γ and contact stress.

Analysis of the behaviour on the varying rail profiles on switches and crossings suggests that the common types of turnouts with vertical rails are unlikely to contribute to the main crack damage band observed on the wheelsets of the monitored fleet. However, very high contact stresses and tangential forces are predicted nearer the flange root and may contribute to other forms of observed damage.

Acknowledgements

This paper describes work undertaken as part of a PhD research program funded by EPSRC through the Rail Research UK Association (RRUKA). The work has also been supported by the Rail Safety and Standards Board (RSSB), Network Rail, Siemens, Alstom, and Bombardier.

References

- [1] Franklin, F. et al: Ratcheting and fatigue-led wear in rail–wheel contact, *Fatigue & Fracture of Eng Mat & Structs* 26, 2003.
- [2] Ekberg, A. et al: An engineering model for prediction of rolling contact fatigue of railway wheels, *Fatigue & Fracture of Eng Mat & Structs* 25, 2002.
- [3] Bernasconi, A. et al: An integrated approach to rolling contact sub-surface fatigue assessment of railway wheels, *Wear* 258, 2005.
- [4] Bevan, A. et al: Development of a wheelset damage model using a combination of wear and rolling contact fatigue prediction, 22nd International symposium of dynamics of vehicles on roads and tracks, IAVSD 2011, Manchester
- [5] Burstow, M: Whole life rail model application and development for RSSB – continued development of an RCF damage parameter, AEATR report AEATR-ES-2004-880 Issue 2, 2004. (Available on www.rssb.co.uk)

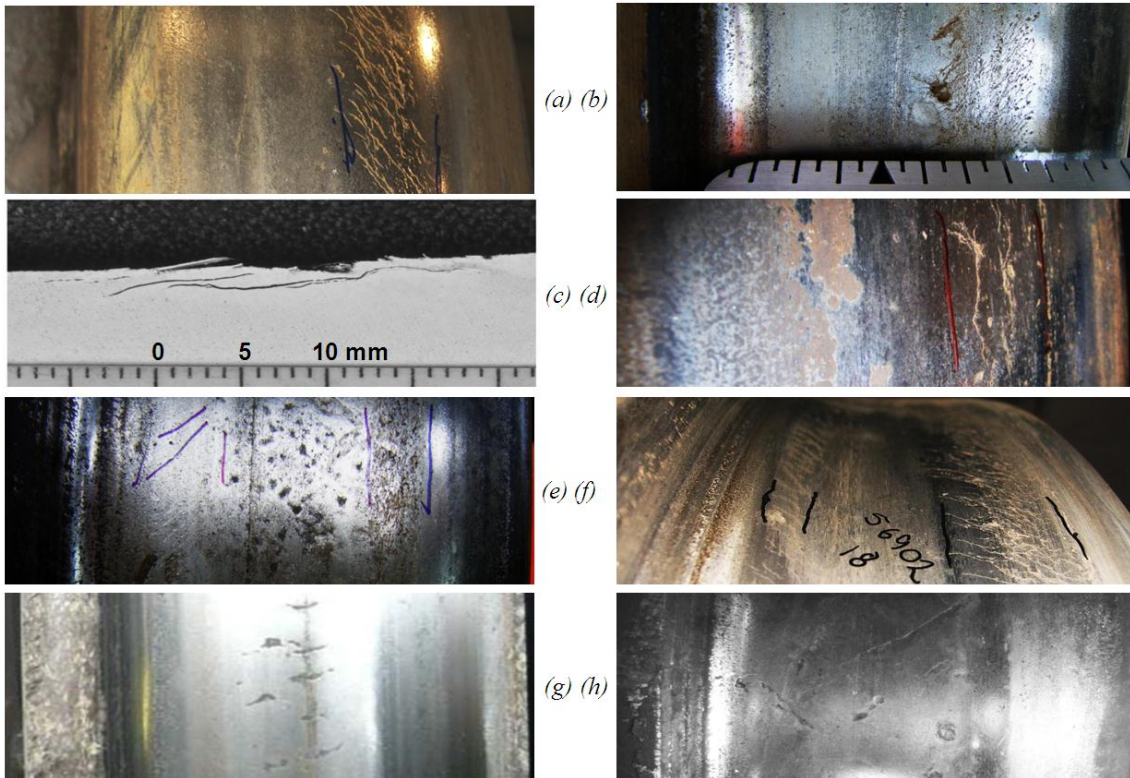


Figure 1: Wheel RCF Observations: (a) angled cracks in field side band, (b) curved cracks with cavities, (c) section showing cracks below surface, (d) circumferential cracks, (e) (f) second band of cracks near flange root, (g) transverse cracks in centre of tread, (h) cracks propagating from indentations.

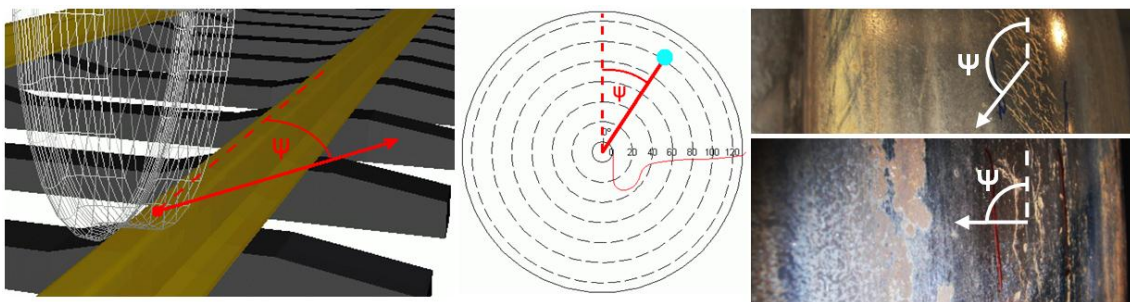


Figure 2: Definition of Datums for Circular Plot

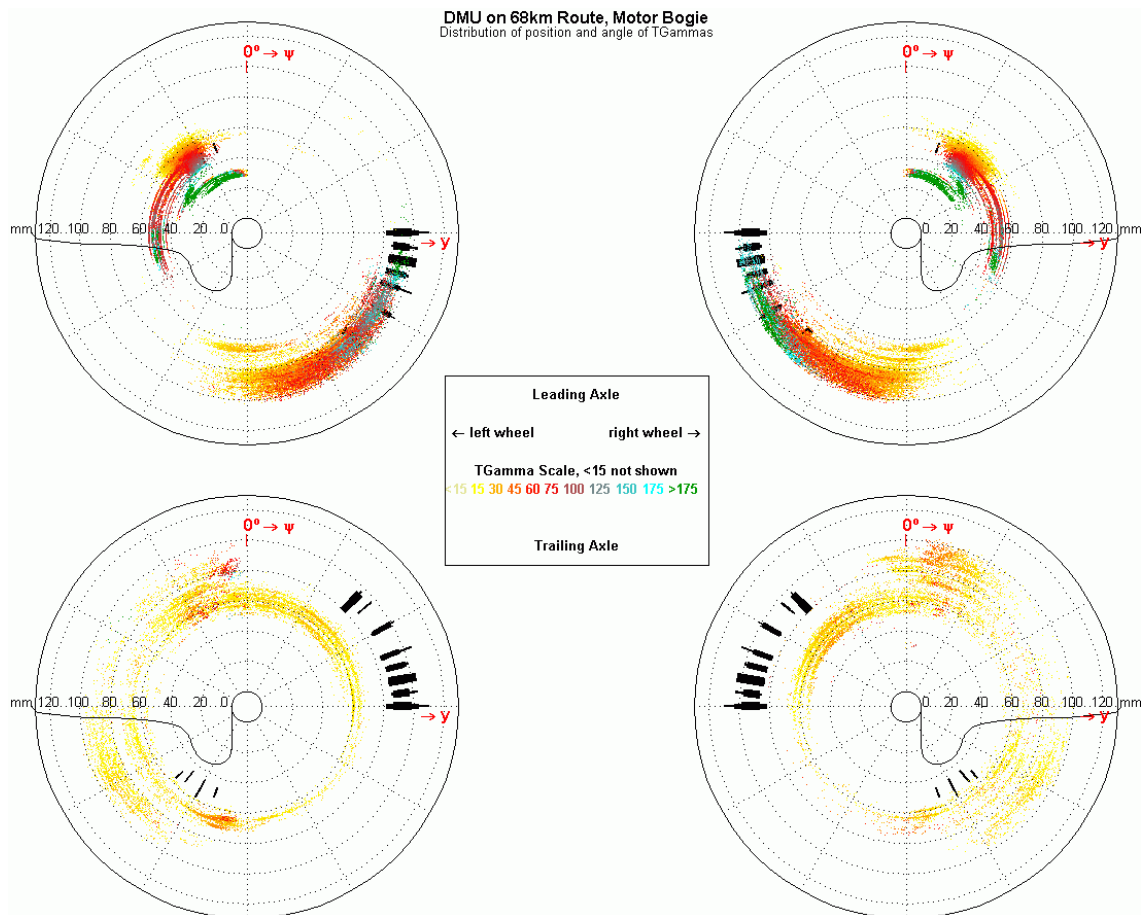


Figure 3: Example Circle Plot, showing contact patch position, creep force angle, $T\gamma$, and observed crack damage for DMU powered bogie operating over a 68km route.

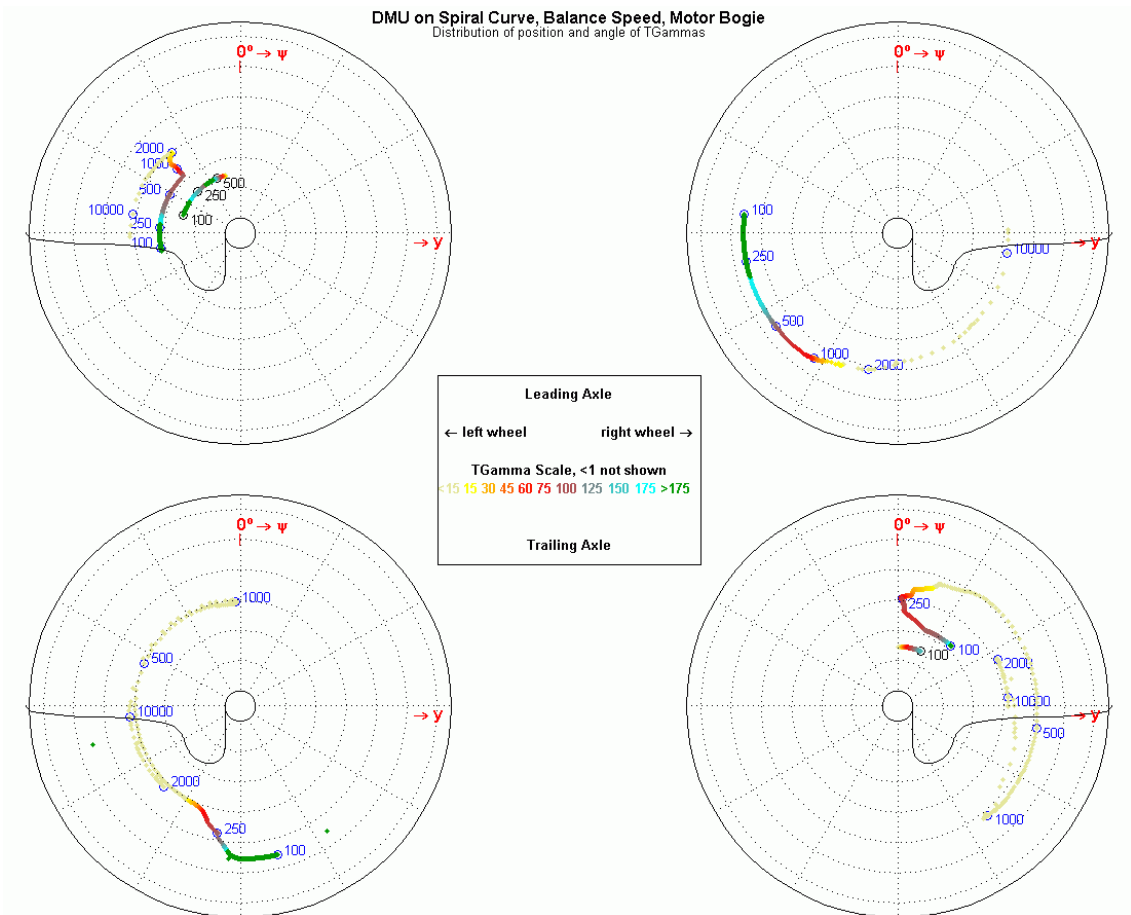


Figure 4: Circle Plot representing running on a right-hand spiral curve at balance speed. Curve radii in metres are annotated in blue (tread contacts) or black (flange contacts).

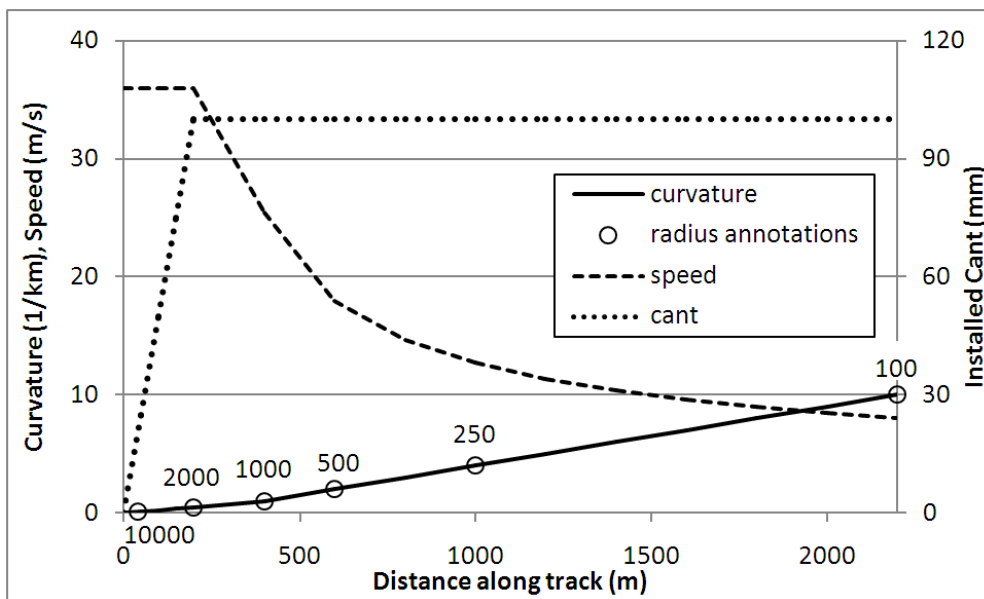


Figure 5: Curvature, cant and speed conditions for right-hand spiral curve analysis at balance speed.

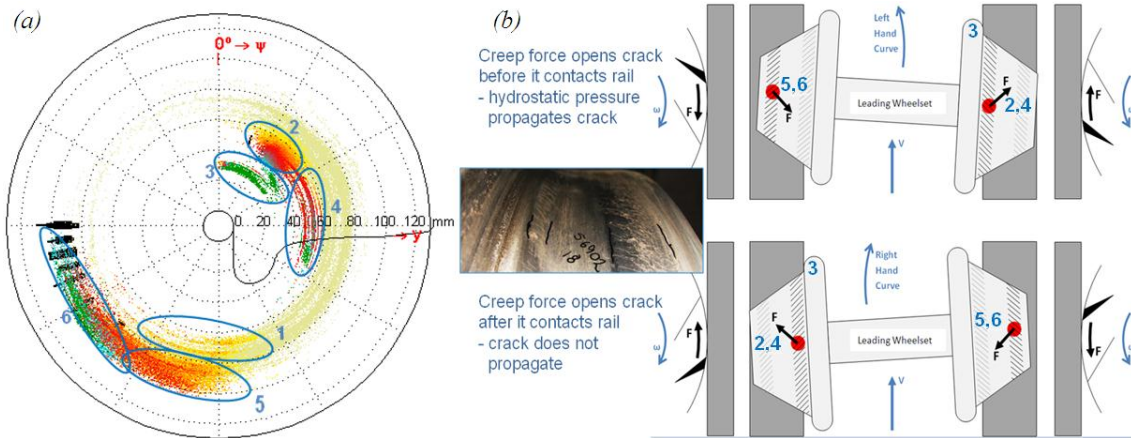


Figure 6: Damage Conditions: (a) Regions on Circular Plot, (b) Wheelset and Crack Orientation

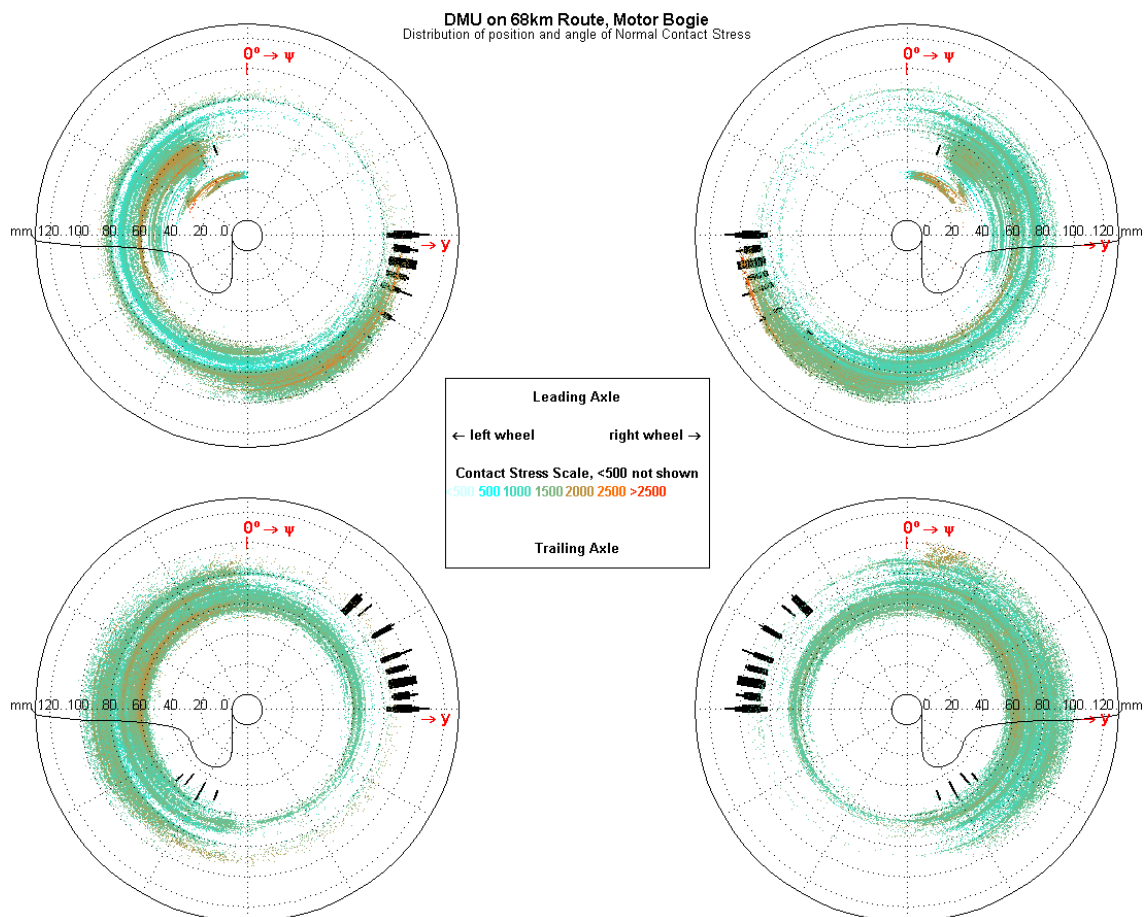


Figure 7: Circle Plot, showing contact patch position, creep force angle, peak contact stress (MPa), and observed crack damage for DMU powered bogie operating over a 68km route.

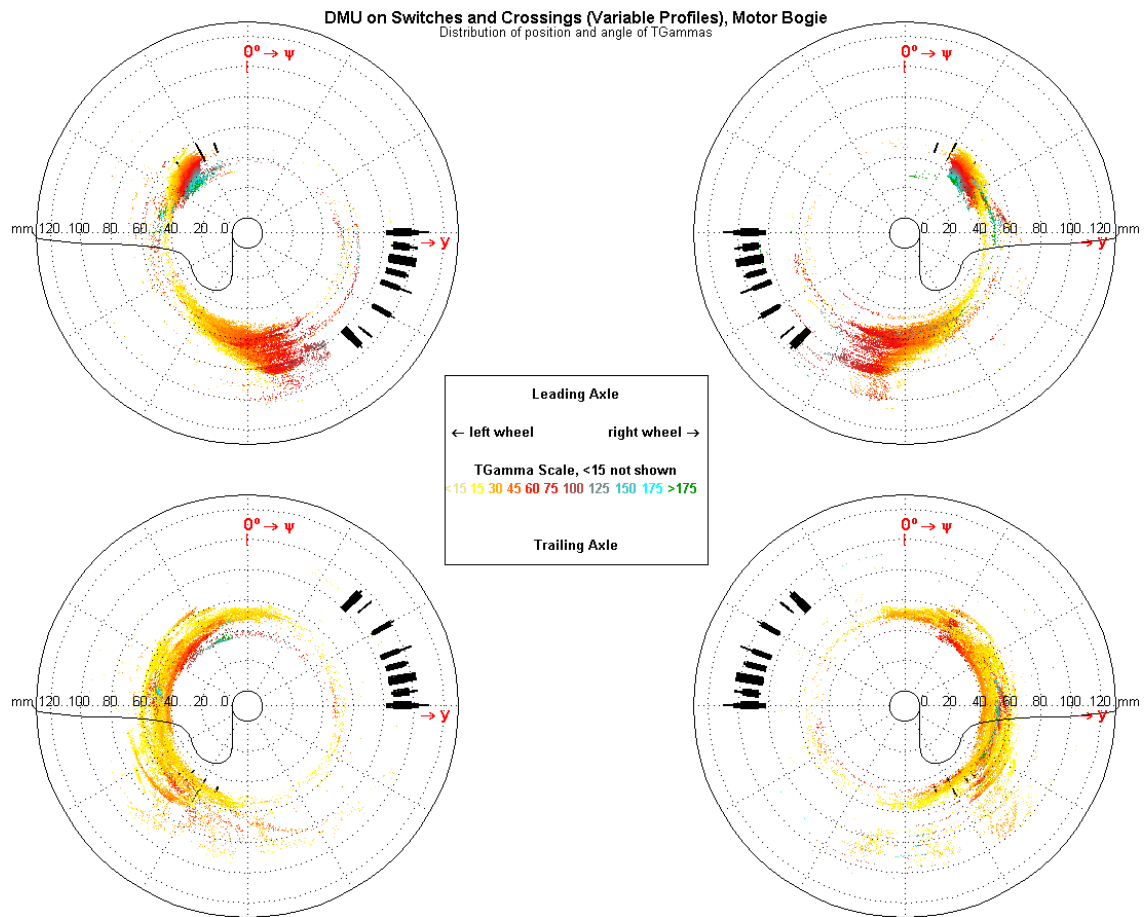


Figure 8: Circle Plot, showing contact patch position, creep force angle, $T\gamma$, and observed crack damage for DMU powered bogie operating over a selection of switches and crossings.

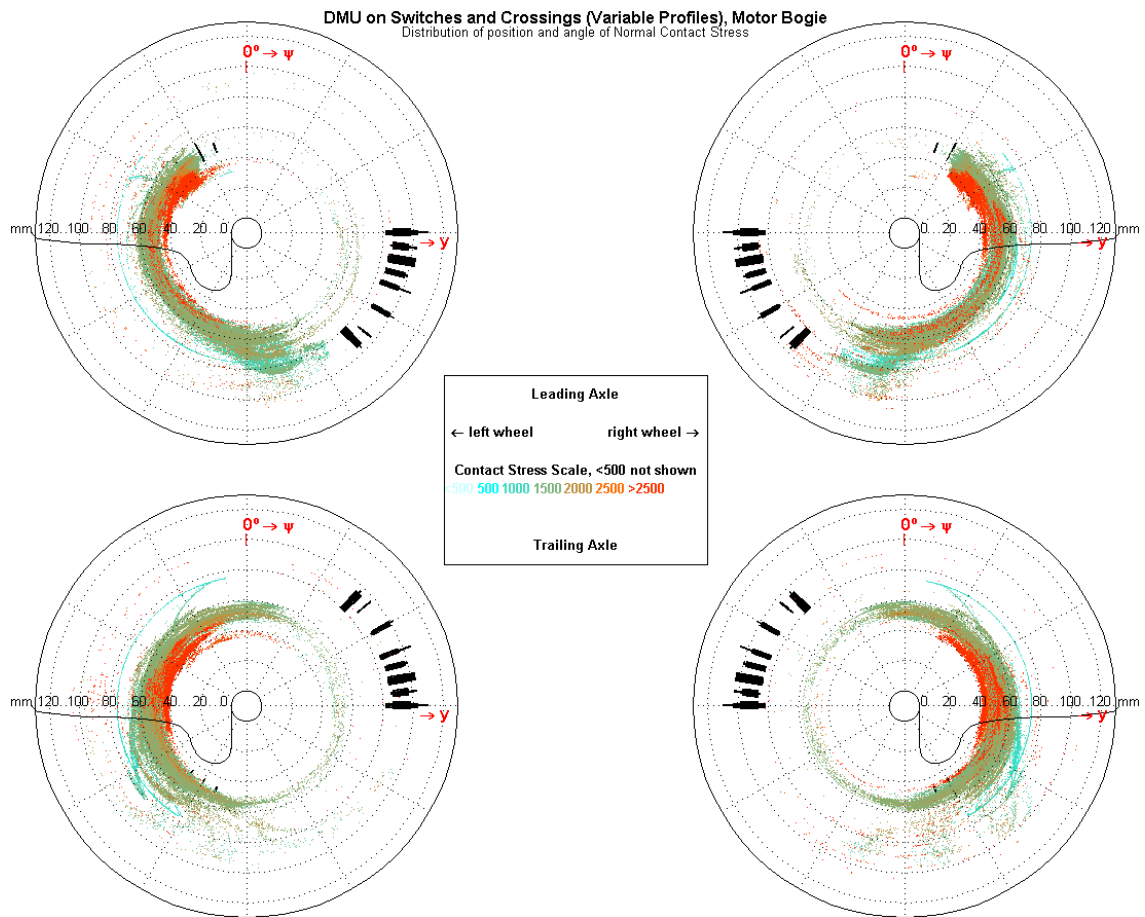


Figure 9: Circle Plot, showing contact patch position, creep force angle, peak contact stress (MPa), and observed crack damage for DMU powered bogie operating over a selection of switches and crossings.